Geotech Geol Eng (2019) 37:431–453
https://doi.org/10.1007/s10706-018-0621-9

ORIGINAL PAPER

Effect of Joint Micro Mechanical Parameters on a Jointed Rock Block Behavior Adjacent to an Underground Excavation: A Particle Flow Approach

Xu-Xu Yang · Pinnaduwa H. S. W. Kulatilake

Received: 28 January 2018 / Accepted: 4 July 2018 / Published online: 7 July 2018

Abstract The particle flow code PFC^{3D} was utilized to investigate mechanical behavior of jointed rock blocks, having non-persistent filled joints, located adjacent to an underground excavation. The focus of this investigation was to study the effect of filled joint micro-mechanical properties on the failure mode and strength of jointed rock blocks by varying the joint orientation. The smooth joint model was incorporated to create non-persistent filled joints having the following micro-mechanical parameters: the joint normal stiffness, joint shear stiffness, bonded joint friction angle, bonded joint cohesion, joint friction coefficient and joint tensile strength. The joint normal and shear stiffness were found to affect the mechanical behavior of jointed rock blocks having joint dip angles less than or equal to 45°. Increase of the bonded joint cohesion increased the strength significantly of jointed blocks having dip angles 30° through 90°. Increase of the bonded joint friction angle increased the strength significantly of jointed blocks having dip angles 30° through 60°. Increase of the joint friction coefficient slightly increased the strength of jointed blocks having dip angles 30° through 60°. Effect of the joint tensile strength on the mechanical behavior of jointed blocks was found to be negligible apart from the jointed block which had 90° dip angle, which showed slight affect. The applied stress path in the conducted study resulted in more shear fractures compared to the tensile fractures in the joint segments. The results indicated the importance of using proper micro-mechanical parameter values to obtain realistic behavior of jointed rock masses in investigating stability of underground excavations using PFC^{3D}.

Keywords Mechanical behavior · Joint micro-mechanical parameters · Jointed rock · Particle flow approach · Underground excavations

1 Introduction

Tunnels excavated in naturally occurring rock masses usually encounter different types of discontinuities. To arrive at safe and economical designs for underground excavations, it is of utmost importance to have a good understanding of the mechanical behavior of rock masses interspaced by those discontinuities. However, the inherent statistical nature of their geometrical parameters as well as their complicated

X.-X. Yang
Shandong Provincial Key Laboratory of Civil Engineering Disaster Prevention and Mitigation, Shandong University of Science and Technology, Qingdao 266590, China

X.-X. Yang · P. H. S. W. Kulatilake (✉)
Rock Mass Modeling and Computational Rock Mechanics Laboratories, University of Arizona, Tucson, AZ 85721, USA
e-mail: kulatila@u.arizona.edu

geomechanical properties makes it difficult to accurately predict the mechanical behavior of rock masses.

The emergence of the particle flow approach is a step forward in numerical modeling of jointed rock masses, and it provides an interesting way to look into effect of joint geometrical and geomechanical properties on rock mass behavior. This approach is implemented in PFC software, and has the capability to track fracture initiation and propagation through intact material and slip/opening occur through pre-existing joints (Potyondy and Cundall 2004; Itasca Consulting Group Inc. 2008; Mars Ivars et al. 2011). The current state-of-the-art on using the particle flow approach has mainly focused on the calibration of micro parameters of the intact material and the influence of geometrical configuration of discontinuities on the rock mass mechanical behavior. Most probably the first comprehensive micro parameter calibration procedure for intact rock was reported by Kulatilake et al. (2001) for PFC^{3D} version 1.1. For the parallel bond, Yang et al. (2015) and Mehranpour and Kulatilake (2016) have given comprehensive procedures to calibrate micro parameters for intact rock. Recently, Chen (2017) and Yin and Meng (2018) also have suggested trial and error procedures to calibrate micro parameters of intact rock. Kulatilake et al. (2001) conducted both physical and PFC^{3D} (version 1.1) (Itasca Consulting Group 1995) modeling on prismatic rock blocks containing a pair of persistent discontinuity sets having fourteen symmetric and non-symmetric dip angle combinations varying between 0° and 45° under uniaxial compression. They observed three failure modes for the jointed blocks having persistent discontinuities: (a) tensile splitting through the intact material, (b) failure by sliding along a joint plane and/or by displacement normal to a joint plane and (c) mixed mode failure involving both the failure mechanisms stated in (a) and (b). Each mode exhibited distinctive features in terms of failure processes along and across discontinuities as well as on the overall deformability and strength of the material. Tien et al. (2006) observed similar failure modes for similar joint configurations in an experimental study conducted under uniaxial compression. Zhao et al. (2015) conducted a particle flow modeling study on the deformation and failure modes of rock blocks containing several parallel joints having different spacing and number. They observed four types of deformation phenomena in the rock blocks, namely, shearing along a single joint, shearing along multiple parallel joints, shearing across joints, and shearing through multiple joints and leading to step-path failure. The jointed rock mass behavior is dependent on the combined directional effect of the joint geometry parameters including the joint density, orientation and size distributions and the number of joint sets (Kulatilake et al. 1993; Wu and Kulatilake 2012).

The existence of rock bridges further complicates the geometric configurations of jointed rock masses (Kim et al. 2007; Wu and Kulatilake 2012), and has led to extensive investigations of mechanical behavior of rock masses having non-persistent joints. Jamil (1992) conducted an experimental study of the effect of joint configuration and loading condition on the failure mode and strength of a rock mass containing non-persistent joints. The parameters investigated were joint orientation with respect to principal stress directions, joint spacing, joint persistence and confining pressure with constant joint step angle of 90°. Prudencio and Van Sint (2007) presented the results of biaxial tests performed on physical models of rock with non-persistent joints. The tests showed three basic failure modes: failure through a planar surface, step-path failure, and failure by rotation of new blocks. Planar failure and step-path failure were associated with moderate strength behavior, and small failure strains, whereas rotational failure was associated with a very low strength, ductile behavior, and a large deformation. Moreover, based on the physical modeling conducted by Prudencio and Van Sint (2007), Bahaaddini et al. (2013) implemented a parametric study using the particle flow method to study the effect of joint orientation, joint persistence, joint spacing, joint step angle and joint aperture on the mechanical properties of jointed rock blocks under uniaxial compression. Five failure modes were identified from the results obtained from this study: intact rock, planar, block rotation, step-path and semi-block generation. Using PFC^{3D}, Zhang and Stead (2014) numerically modeled 3D crack propagation in hard rock pillars. Zhang and Wong (2012), using PFC^{2D}, investigated the cracking processes in rock-like material containing a single flaw under uniaxial compression, and confirmed the strong influence of pre-existing flaw on the crack initiation and propagation patterns. Ghazvinian et al. (2012) adopted PFC^{2D} to simulate the shear behavior of rock-like material samples containing planar non-persistent joints and

investigated the effect of joint separation on the failure behavior of rock bridges. In a follow up study, Sarfarazi et al. (2014) further investigated the effect of joint overlap on the full failure behavior of a rock bridge in the shear-box test by means of particle flow code in two dimensions. The above-mentioned research shed lights on the understanding of the effect of joint geometry on the mechanical behavior of jointed rock masses.

However, the influence of joint mechanical properties on the global response of jointed rock masses, especially with non-persistent discontinuities, is not clear yet. As a matter of fact, the weathering as well as different conditions of closed joints with infill or cementing material between the joint surfaces produce a wide range of mechanical properties, which further influence the rock mass behavior. Barton et al. (1985) proposed a model to describe the shear strength of joints incorporating the effect of roughness, wall strength, aperture, filling and seepage. Indraratna et al. (2001) investigated the behavior of joints containing clay infill under constant normal stiffness and demonstrated a significant reduction in shear strength when the joint contained a layer of clay infill of 1.5 mm. Fan et al. (2015), through a particle mechanics approach, studied the mechanical behavior of rock-like jointed blocks with multi-non-persistent joints under uniaxial loading. They found that the joint particle stiffness plays a minor to a significant role on the uniaxial compression strength and plays a negligible to a moderate role on the deformation modulus which depends on the joint orientation and joint persistence. Yang et al. (2015), using PFC^{3D}, also observed that the joint normal stiffness, joint shear stiffness and joint friction coefficient induced changes on strength of jointed rock blocks having dip angles of 30°, 45° and 60°. Recently, Bahaaddini et al. (2015) conducted a parametric study of joint parameters on the shear behavior of rock joints and found that the joint normal stiffness and joint shear stiffness have insignificant effect on the peak shear strength in the sliding mode, but that the joint normal stiffness has a significant effect on the dilation rate in both the sliding and shearing modes. Huang et al. (2015) reported a numerical study on the effects of micro-parameters of the smooth joint model including the joint stiffness and friction coefficient on the macro-properties and the associated failure models of synthetic rock masses under the uniaxial compression condition. Recently, Hu et al. (2018) carried out an investigation on the effect of smooth joint parameters on the macroscopic properties and failure mechanism of jointed rock under triaxial compression test. Mehranpour and Kulatilake (2017) reported two shortcomings of the smooth joint model and suggested procedures to overcome them. Even though some progress has been made, understanding of the effect of each micro-parameter of smooth joint model on the global behavior of rock mass is still not clear. Note that the above-mentioned studies have not been performed on infilled joints even though those were conducted on closed joints. Moreover, those studies mainly simulated the laboratory loading conditions. The effect of infilled joint micro parameters on the rock mass behavior incorporating large physical models subjected to excavation-induced stress paths have not been investigated.

In the present paper, the PFC^{3D} software package (version 4.0) (Itasca Consulting Group Inc. 2008) is utilized to establish a numerical model for the large scale physical model proposed by Zhang (2013) and Jing et al. (2014) to thoroughly investigate the effect of joint micro-mechanical parameters on jointed rock block behavior adjacent to an underground excavation. The studied joints are closed with bonded strength to simulate the infilled joints, thus incorporating joint normal stiffness, joint shear stiffness, bonded joint friction angle, bonded joint cohesion, joint friction coefficient, and joint tensile strength. The authors are not aware of any previous study conducted to investigate the effect of infilled joints on jointed rock block behavior adjacent to an underground excavation incorporating both large scale physical modeling and PFC^{3D} numerical modeling. By varying the above-mentioned joint micro-mechanical parameter values, the failure modes and normalized strength of rock blocks having non-persistent joints were systematically studied. Furthermore, the effect of joint shear and slip response on the mechanical behavior of jointed rock blocks adjacent to an underground excavation was also analyzed. The numerical modeling results provide useful guidelines with respect to stability of underground excavations.

2 Setting Up of Jointed Rock Block Models for Particle Flow Simulation

2.1 Setup of a Jointed Rock Block Model

The setup of the numerical model studied in this paper is based on a physical rock block model proposed by Zhang (2013) and Jing et al. (2014). Their model was aimed at obtaining a better understanding of the mechanical behavior of jointed rock blocks located adjacent to an excavation in an underground coal mine. Figure 1 shows the selected jointed rock block located adjacent to an underground coal mine excavation. The selected jointed rock block of size 2.5 m × 2.5 m × 2.4 m has a free surface as part of the underground excavation wall without any rock support. Figure 2 displays the conceptual rock block model and the corresponding synthetic rock block model used in the large scale physical experiment (Zhang 2013; Jing et al. 2014). As shown in Fig. 2a, the major principal stress, σ_1, acts in the vertical direction (along the y axis). The intermediate principal stress, σ_2, acts in the lateral direction along the x axis. Along the z axis the rear surface is fixed with no movement, while the front surface is set to be free without any constraints applied on it. Therefore, the front surface is called the free surface. In the physical experiment, a specially designed loading frame has been used to apply the aforesaid stress system (Fig. 2a) on a synthetic jointed rock block of the size 0.5 m × 0.5 m × 0.48 m (Fig. 2b). The synthetic jointed rock block was fabricated by mixing C42.5 cement, plaster, silica flour in the mass ratio of 7:3:5:2.5. Note that this is a good simulant to coal measure rocks which can be categorized under soft rocks. The unit weight of the synthetic rock-like sample was 16.35 kN/m^3. The uniaxial compressive strength, UCS, and the elastic modulus, E, determined by conducting unconfined compression tests on cylindrical specimens of diameter 50 mm and height 100 mm in the laboratory for the synthetic rock material were 3.77 MPa and 0.44 GPa, respectively. In fabricating the synthetic rock block using a mould, nine joints were arranged in an en echelon pattern by inserting steel plates of thickness 2 mm and width 100 mm through the model along the σ_2 direction. The length of each joint was 100 mm with the intact material bridge length of 100 mm. The distance between two adjacent joints was 100 mm. The above-mentioned specimens then were carefully cured in water under 20 ± 5 °C temperature for 7 days before pulling out the steel plates to create the joints. After another 8 days, the moulds have been removed and then the joints have been filled with talcum powder and plugged with plaster to simulate smooth joints. Before testing, the specimens were cured for 60 days in water. For further details on the physical experiment the reader is referred to Zhang (2013) and Jing et al. (2014). In each test, σ_1 was increased under a constant σ_2 until the sample failed.

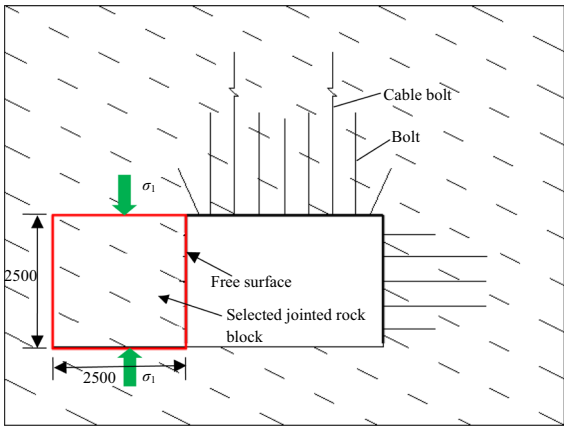

Fig. 1 Selected jointed rock block located adjacent to an underground excavation (unit: mm)

A particle flow model of a jointed rock block of the same size as that of the physical experiment was created by using the PFC^{3D} software package as shown in Fig. 3. In this numerical model, the rear wall and bottom wall were restrained moving in the lateral (z direction) and vertical directions, respectively. The velocity of the other two lateral walls in the x direction were controlled by a servo-control mechanism to maintain a certain confining stress, σ_2 = 1.15 MPa as applied in the physical experiment (Zhang 2013; Jing et al. 2014). During the numerical compression test, the rock block models were loaded by the top wall having a constant velocity. Besides the aforesaid five walls, a front wall was also created to form a vessel for generation of the synthetic rock material. After the whole model was set to be in static state under a uniform pressure of 1.15 MPa by moving the four movable walls, the front wall was then deleted to expose a free surface to simulate the unsupported inner face of the underground excavation.

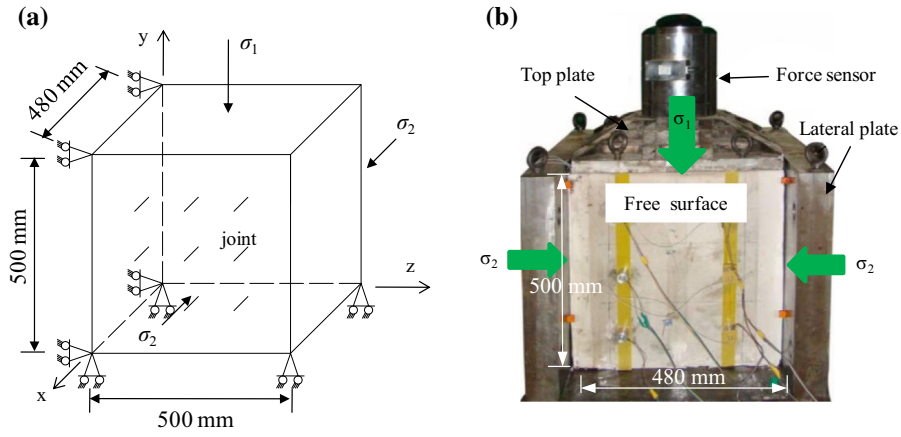

Fig. 2 **a** Conceptual jointed rock block model; **b** synthetic jointed rock block model used for the physical experiments. Reproduced with permission from Zhang (2013) and Jing et al. (2014)

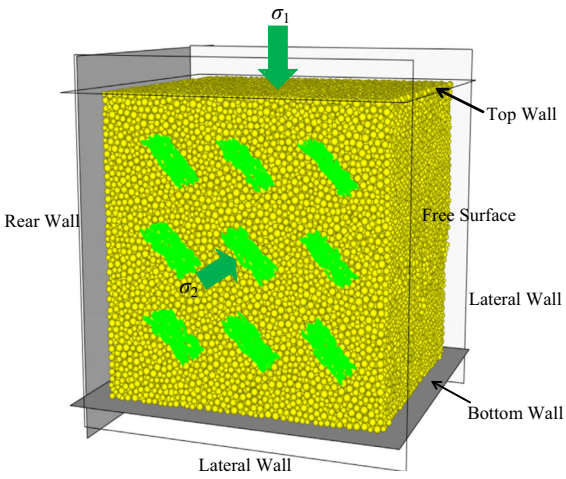

Fig. 3 Particle flow model of the synthetic jointed rock block created with the PFC^{3D} software

The intact material in the synthetic jointed rock block model (Fig. 3) is represented by the parallel bond model (Potyondy and Cundall 2004; Itasca Consulting Group Inc. 2008; Mars Ivars et al. 2011). The parallel bond can be envisioned as a set of elastic springs uniformly distributed over a rectangular cross-section lying on the contact plane and centered at the contact point. Parallel bonds can transmit not only the force but also the moment between particles. Thus, the parallel bond model is commonly used to mimic rock-like materials (Lee and Jeon 2011; Zhang and Wong 2013). To represent the mechanical properties of the rock-like material used in the physical experiment (Zhang 2013; Jing et al. 2014), the particle flow modeling approach requires selection of the basic micro-mechanical parameter values to describe the contact stiffness, bond stiffness, bond strength and contact friction. Therefore, a calibration procedure was implemented to determine these micro-mechanical parameter values for the intact material. A few steps were followed to reproduce several properties, such as the UCS, Young's modulus and Poisson's ratio, of the physical experimental material (Yang et al. 2006, 2015). Table 1 lists the calibrated micro-mechanical parameter values obtained for the intact material. The comparison between the numerical and experimental results given in Table 2 demonstrates the capability of the particle flow model in reproducing the rock-like material properties.

2.2 Smooth Joint Model

After the vessel formed by the six walls was filled with particles cemented by the parallel bonds, the smooth joint model (Itasca Consulting Group Inc. 2008) was utilized to create a non-persistent joint set as shown in Fig. 4. When modeling the joint surface with the particle flow code, the interfaces represented by the debonding contacts along a line or plane would result in inherent roughness (Potyondy and Cundall 2004; Itasca Consulting Group Inc. 2008; Mars Ivars et al. 2011). This roughness can lead to unrealistic increases in shear strength as well as dilation during shearing along the joint plane (Kulatilake et al. 2001; Bahaaddini et al. 2012). The smooth joint model was proposed to get rid of the aforesaid roughness.

The smooth joint contact model is shown in Fig. 4. Once a joint plane is defined, a smooth joint is assigned at the contacts between balls whose centers are located on the opposite sides of the designed joint

Table 1 Micro-mechanical parameter values used for the intact material

Parameter of particle	Value	Parameter of parallel bond	Value
ρ (kg/m^3)	1635	λ	1.0
k_n/k_s	1.70	$\overline{k}_n/\overline{k}_s$	1.70
E_c (GPa)	0.37	$\overline{E}_c$ (GPa)	0.37
μ	0.60	$\overline{\sigma}_c$ [mean ± SD (MPa)]	3.00 ± 0.75
$R_{rat} = R_{\max}/R_{\min}$	1.66	$\overline{\tau}_c$ [mean ± SD (MPa)]	3.00 ± 0.75
R (m)	$R_{\max} = 1.079 \times 10^{-3}$, $R_{avg} = 0.865 \times 10^{-3}$, $R_{\min} = 0.650 \times 10^{-3}$ (for cylindrical specimen)		
	$R_{\max} = 7.280 \times 10^{-3}$, $R_{avg} = 5.915 \times 10^{-3}$, $R_{\min} = 4.550 \times 10^{-3}$ (for jointed rock block)		

ρ is the density of the synthetic rock material; λ is the radius multiplier used to set the parallel bond radii; R is the radius of the particle; $R_{\max}$, R_{avg} and $R_{\min}$ are the maximum radius, average radius and minimum radius of the particle, respectively

Table 2 Comparison between the numerical and experimental results

Mechanical parameter	Numerical simulation result	Laboratory experimental result	Deviation
σ_c/MPa	3.78	3.77	0.3%
E/GPa	0.433	0.440	1.6%
v	0.185	0.160–0.250	N/A

The Poisson's ratio, v, in the laboratory experimental result is not obtained by the experiment; it is calculated according to a similarity criterion (Zhang 2013; Jing et al. 2014)

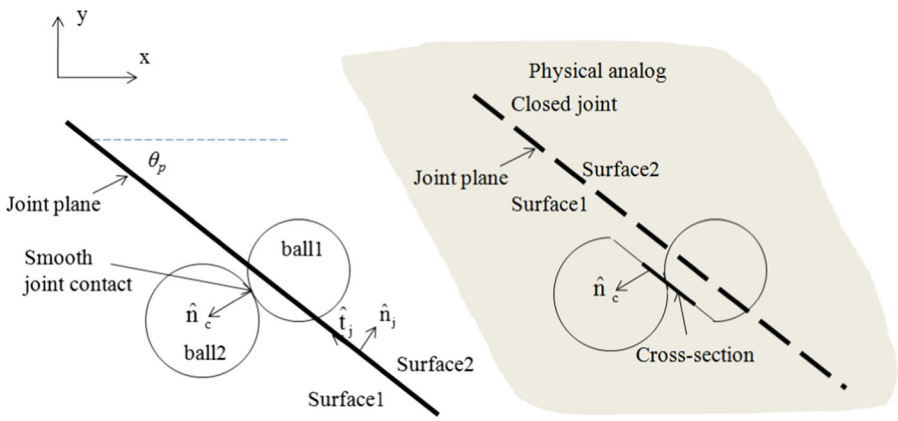

Fig. 4 Smooth joint contact model. Reproduced with permission from Itasca Consulting Group Inc. (2008)

plane. At these contacts, first, the existing bonds are removed, and smooth joints are defined in a direction parallel to the joint plane regardless of the contact orientations. These contacts behave according to the rules followed by the smooth joint model with specified parameters given by the user. The particles having such contacts may overlap or pass through each other rather than be forced to roll around one another.

The smooth joint model can be applied under four basic modes: (a) not bonded and never fail mode; (b) not bonded and fail in tension mode; (c) not bonded and fail in shear mode; (d) bonded mode. With these

four modes, the smooth joint model can be used to mimic different joint conditions. Herein, we use the joint under the bonded mode to simulate a joint with a cemented filling material or grout. Therefore, the smooth joint mechanical parameters include the normal stiffness, $\overline{k}_{nj}$, shear stiffness, $\overline{k}_{sj}$, tensile strength, $\overline{\sigma}_{cj}$, shear strength, $\overline{\tau}_{cj}$, and coefficient of friction, μ_j.

The behavior of the bonded smooth joint model can be described through the schematic given in Fig. 5. Between the two joint surfaces there are two sets of springs to provide the normal stiffness and shear stiffness. Besides, the bonded joint model has both the normal and shear strength. The shear strength follows the Coulomb criterion as given in Eq. 1:

$$\overline{\tau}_{cj} = \overline{\sigma}_{nj} \tan \varphi_j + c_j. \quad (1)$$

In Eq. 1, $\overline{\sigma}_{nj}$ is the normal stress applied on the joint surface (in MPa); φ_j is the bonded joint friction angle (in deg.) and c_j is the bonded joint cohesion (in MPa). When the normal or shear stress exceeds the bond strength, the bond between the two joint surfaces is broken and the bond stiffness gets removed. Once the parallel bond breaks either in shear or tensile mode, the shear strength falls to its residual value and the tensile strength is set to zero. The residual shear strength is dependent on the normal stress, $\overline{\sigma}_{nj}$, and the joint friction coefficient, μ_j. Figure 6 displays the force–displacement law for a bonded smooth joint.

In this paper, the following joint micro mechanical parameters: normal stiffness, $\overline{k}_{nj}$, shear stiffness, $\overline{k}_{sj}$, tensile strength, $\overline{\sigma}_{cj}$, bonded joint friction angle, φ_j, bonded joint cohesion, c_j, and coefficient of friction, μ_j are varied systematically to study their effect on the failure mode and the strength of a jointed rock block located adjacent to an underground excavation.

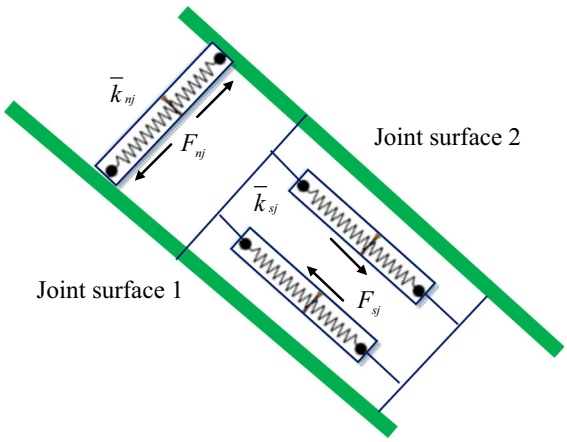

Fig. 5 A schematic for the bonded smooth joint model

3 Effect of Joint Properties on Jointed Rock Block Behavior

To investigate the effect of joint micro-mechanical parameters on the failure mode and strength behavior of rock blocks having non-persistent joints, a parametric study was carried out using PFC^{3D} based on the developed numerical model (Fig. 3). Due to the significant effect of the joint orientation on the jointed rock mass behavior (Kulatilake et al. 1993; Lee and Jeon 2011; Wu and Kulatilake 2012; Zhang and Wong 2013), in the following sections the effect of each joint micro-mechanical parameter is investigated for a range of values of joint dip angle, α, from 0° to 90° at an interval of 15° (Fig. 7). The jointed blocks having different joint orientations are numerically simulated under compression. Moreover, for better understanding of the effect of non-persistent joints on the rock block model behavior, an intact rock block model with no joints was numerically simulated first. Figure 8 shows the failure process of the intact rock block model. Note that the red implies the tensile cracks, and the blue implies the shear cracks. Cracks are shown on a cross section parallel to the $\sigma_1 - \sigma_3$ plane. The variation of that in the σ_2 direction is negligible. As can be seen from Fig. 8, the fractures initiate from the top of the model adjacent to the free surface, and generally propagate down towards the inner part of the rock block model. The free surface has a significant influence on the failure process of the rock block around the underground excavation. Herein, this kind of failure mode occurring in the intact rock block model is referred to as the *Intact material failure*. The strength of the synthetic intact rock block model under compression was found to be 5.17 MPa.

According to the numerical modeling results of the synthetic jointed rock block models, four failure modes were identified in the conducted compression tests (Fig. 9): (a) *Intact material failure* This failure mode not only happens in the synthetic intact rock block model, but also happens in a few of the synthetic

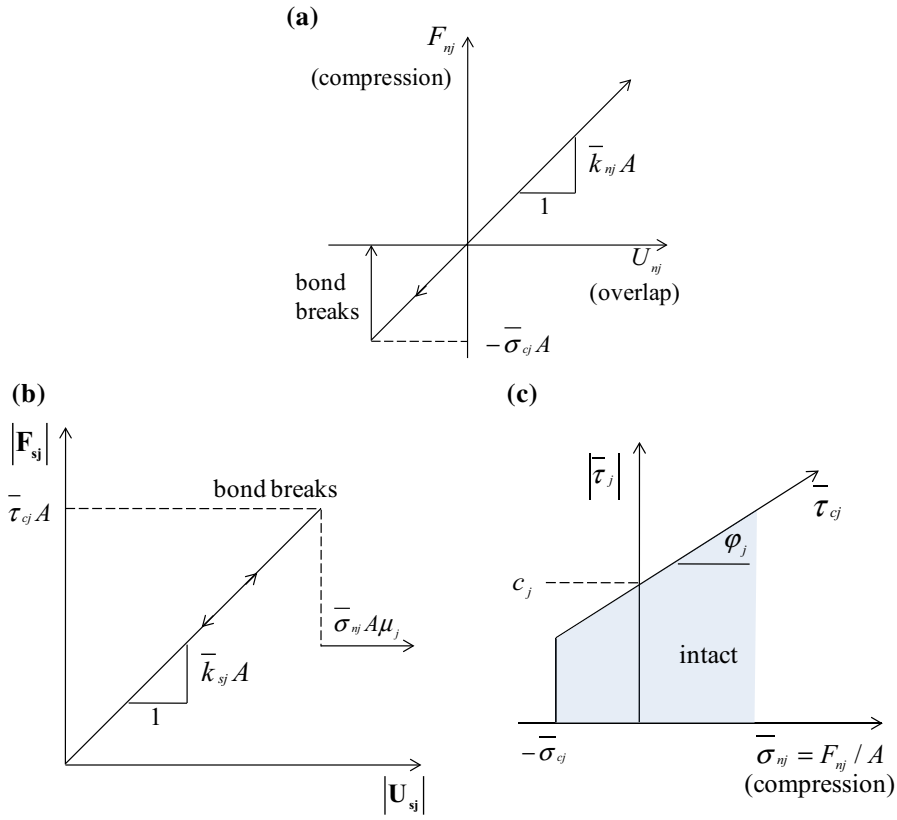

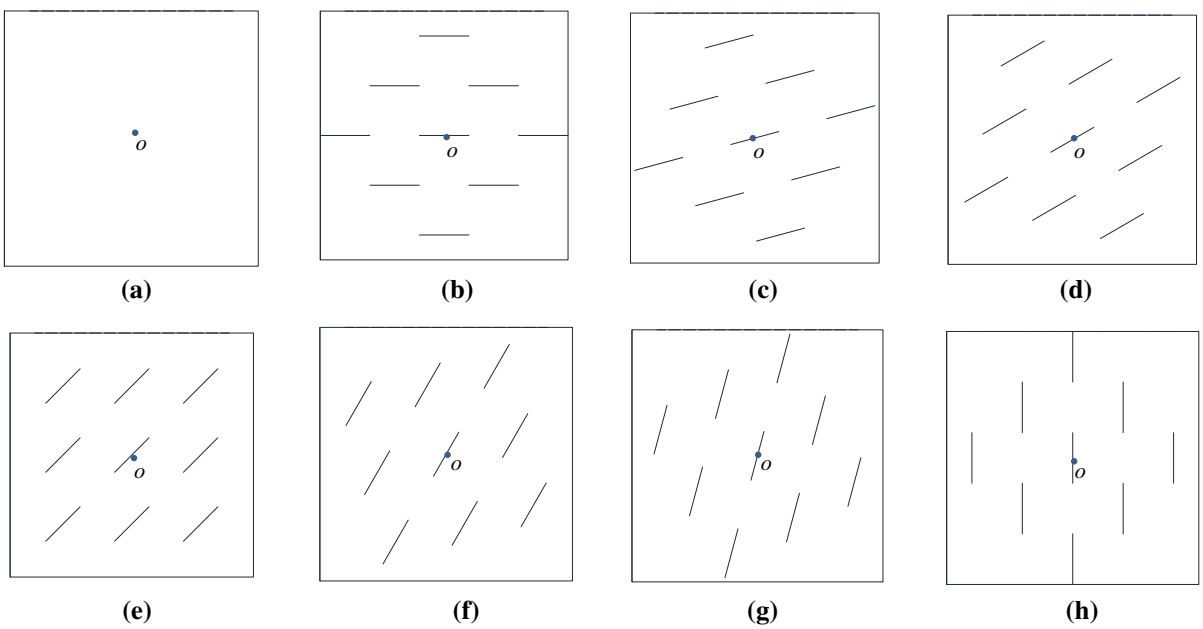

Fig. 6 Force–displacement law for a bonded smooth joint: **a** normal force versus normal displacement; **b** shear force versus shear displacement; **c** strength envelope. Reproduced with permission from Itasca Consulting Group Inc. (2008)

Fig. 7 Jointed rock models having different dip angle (*o* implies the center of the whole model). **a** No joint. **b** $\alpha = 0°$. **c** $\alpha = 15°$. **d** $\alpha = 30°$. **e** $\alpha = 45°$. **f** $\alpha = 60°$. **g** $\alpha = 75°$. **h** $\alpha = 90°$

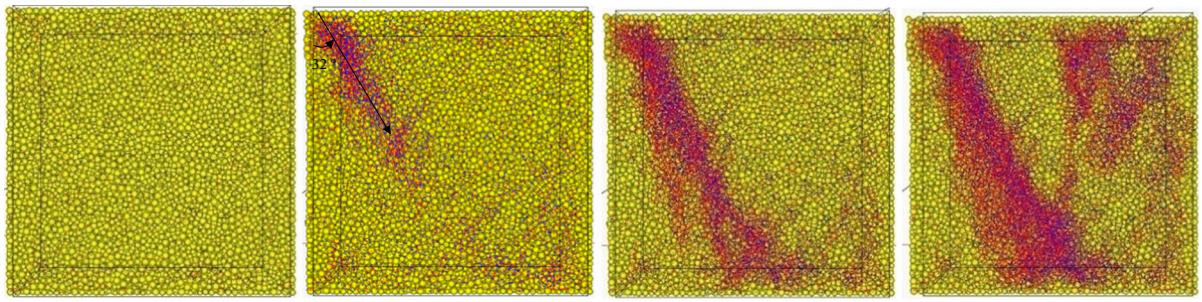

Fig. 8 Failure process of the synthetic intact rock block model from numerical simulation. (Note that the free surface is on the left-hand side of each block.)

jointed rock block models where the joints play a negligible role on the rock mass failure behavior. (b) *Splitting failure* This failure mode also can be considered as one type of *Intact material failure*. In this mode, the fractures develop and coalesce from one joint tip to another joint middle or tip of the parallel set, and the ultimate failure plane in this mode is perpendicular to the joints and approximately along the loading direction. (c) *Step-path failure* This failure mode occurs through sliding on a joint segment and fracturing through the intact material that exist between adjacent parallel joints. In this failure mode, the bond breakages initiate from a joint tip and develop to another joint tip of the parallel set at the opposite side. (d) *Planar failure* The fractures develop along a joint set and the intervening rock bridges and coalesce into a single failure plane having the same dip as the joints. The bond breakages initiate from the joint tips and propagate through the rock bridges until it reaches the adjacent joint tip.

3.1 Effect of Joint Normal Stiffness, $\overline{k}_{nj}$, on Mechanical Behavior of Jointed Rock Blocks

To investigate the effect of joint normal stiffness, $\overline{k}_{nj}$, on mechanical behavior of jointed rock blocks adjacent to an underground excavation, the joint normal stiffness value was varied from 1.36×10^{10} N/m^3 to 1.36×10^{8} N/m^3 through 1.36×10^{9} N/m^3. The joint shear stiffness, $\overline{k}_{sj}$, was also changed with the joint normal stiffness to maintain the shear to normal stiffness ratio equal to 1/3 ($\overline{k}_{sj}/\overline{k}_{nj} = 1/3$); the other joint micro-mechanical parameters were kept constant, i.e. $\overline{\sigma}_{cj} = 0.5$ MPa, $\varphi_j = 20°$, $c_j = 0.5$ MPa, and $\mu_j = 0.3$. Figures 9 and 10 shows, respectively, the failure mode and strength of the synthetic jointed rock blocks having different joint normal stiffness. Note that the strength of the jointed rock blocks was normalized by that of the intact rock block strength of 5.17 MPa.

As can be seen from Figs. 9 and 10, both the failure mode and strength of the jointed rock blocks are influenced heavily by the joint orientation at each joint normal stiffness level. Furthermore, the joint normal stiffness has major influence on the mechanical behavior of the jointed rock blocks having the same joint dip angle. Specifically, when the joint normal stiffness is high ($\overline{k}_{nj} = 1.36 \times 10^{10}$ N/m^3), the highest strength occurs at dip angle of 0°, which is as much as 97.7% of the intact rock block strength. At α = 15°, the strength value is also quite high, 97.5% of the intact rock block strength. That is because in this case ($\overline{k}_{nj} = 1.36 \times 10^{10}$ N/m^3), when the dip angle is small (α = 0° and 15°), the jointed rock block fails in the mode of intact material failure, which is like that happens in the intact rock block. The fractures (failure planes) initiate from the top of the model adjacent to the free surface and propagate downwards into the inner part of the rock block model regardless of the pre-existing joints. However, as the joint normal stiffness decreases, the failure mode as well as the strength of the jointed rock blocks with α = 0° and 15° change dramatically. At α = 0°, with the decrease of joint normal stiffness from 1.36×10^{10} N/m^3 to 1.36×10^{8} N/m^3, the failure mode changes from the intact failure to splitting failure. Compared to the intact failure mode, the splitting failure mode resulted in more macro failure planes extensively distributed in the jointed rock block model. Accordingly, the strength of the jointed rock block failing in splitting

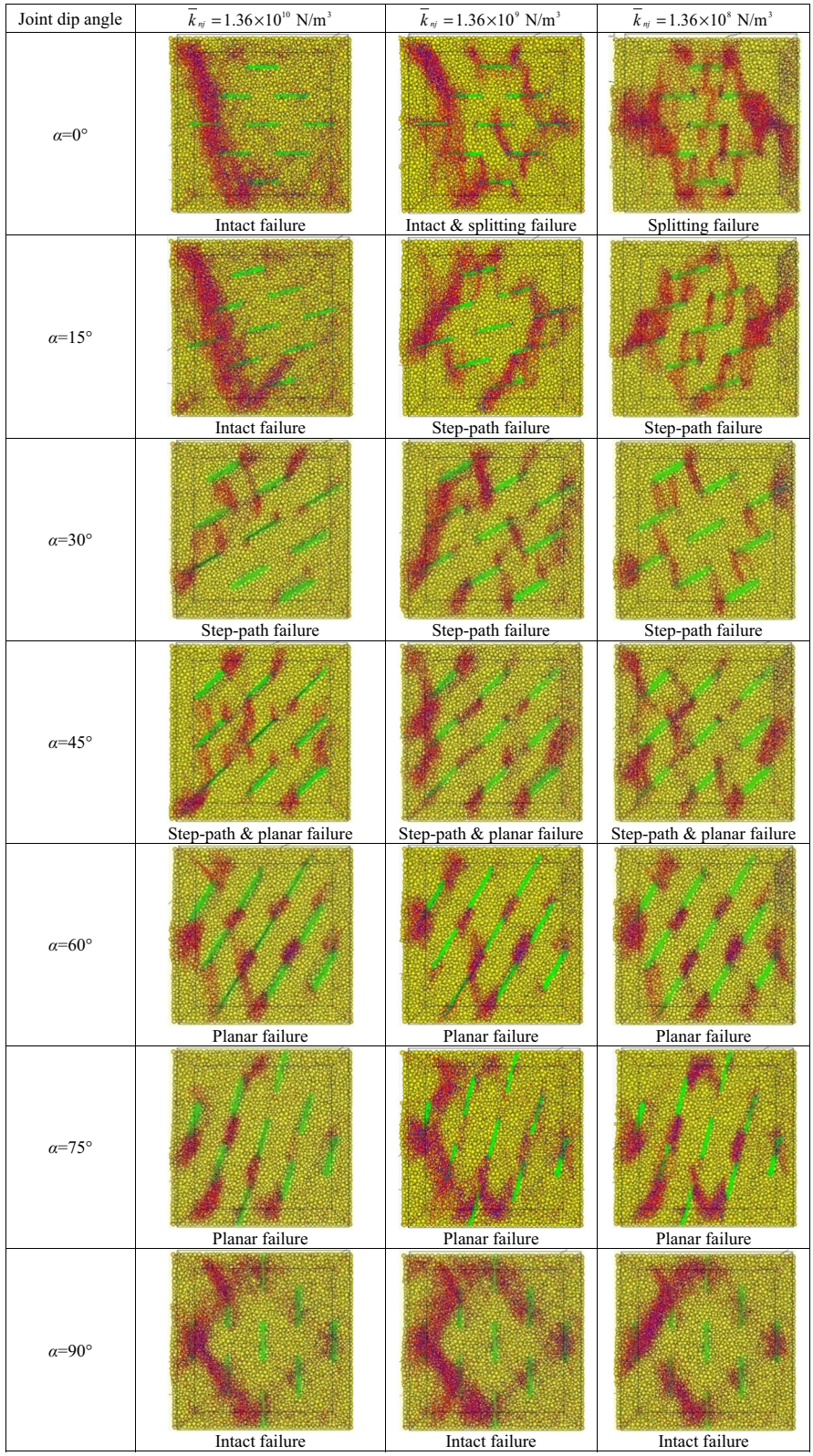

Fig. 9 Failure modes of the synthetic jointed rock blocks having different joint dip angles and joint normal stiffness. (Note that the free surface is on the left-hand side of each block.)

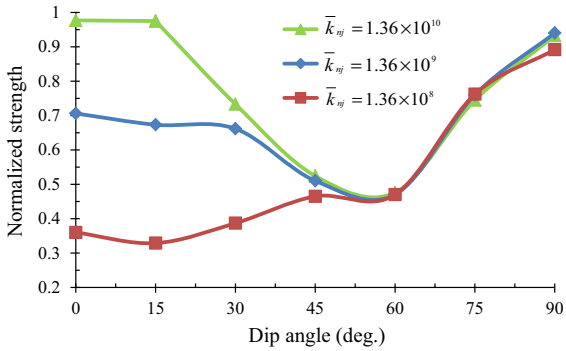

Fig. 10 Normalized strength of the synthetic jointed rock blocks having different joint normal stiffness. (Note that the unit for joint normal stiffness is N/m^3.)

failure mode is much lower than that of the jointed rock block failing in the intact failure mode (only 35.9% of the intact rock block strength), as shown in Fig. 10. At $\overline{k}_{nj} = 1.36 \times 10^9$ N/m^3, the jointed rock block fails in a mixed mode of intact and splitting failure, and the normalized strength is 0.706. At $\alpha = 15°$, with the decrease of joint normal stiffness from 1.36×10^{10} N/m^3 to 1.36×10^8 N/m^3 through 1.36×10^9 N/m^3, the failure mode changes from intact failure to step-path failure and the normalized strength of these jointed rock blocks are 0.975, 0.673 and 0.329, respectively.

When the joint dip angle is greater than 30°, the variation of the joint normal stiffness does not influence significantly the failure mode of the jointed rock block for each dip angle value. The joint orientation plays a dominant role on the failure behavior of the jointed rock block models; for example, at $\alpha = 30°$, 60° and 90° the jointed rock blocks show step-path failure mode, planar failure mode and intact failure mode, respectively (Fig. 9). Nevertheless, at $\alpha = 30°$ and 45° the jointed rock block strength still shows a reducing trend with the decrease of the normal stiffness, even though the extent is less significant. For high dip angles ($\alpha = 60°$, 75° and 90°), negligible difference happens on both the failure mode and strength of the jointed blocks with respect to the variation of the joint normal stiffness (Fig. 10).

In particle flow modeling, it is of interest to see whether a good agreement can be obtained between the numerical simulations and laboratory physical experiment results. From Table 2, a good agreement was achieved on the synthetic intact material in terms of the strength and deformation parameter values. Figure 11 displays the comparison of the synthetic jointed rock block strength obtained between the laboratory physical experiment and numerical modeling results. Note that in the laboratory physical experiments (Zhang 2013; Jing et al. 2014) strength values of the jointed rock blocks are available only for $\alpha = 30°$, 45° and 60°. As shown in Fig. 11, the numerically determined strength values vary around that determined through the laboratory physical experiments for $\alpha = 30°$, 45° and 60°. By selecting the appropriate joint parameter values, example: $\overline{k}_{nj} = 1.36 \times 10^{10}$ N/m^3 in this case, the deviations of the strength between the laboratory physical experiments and numerical simulations are 2.7, 7.5 and 7.9% for $\alpha = 30°$, 45° and 60°, respectively. That means with respect to the strength of the jointed rock blocks, the numerical modeling results (Yang et al. 2015) agreed well with that of the laboratory physical experiments (Zhang 2013; Jing et al. 2014).

3.2 Effect of Joint Shear Stiffness, $\overline{k}_{sj}$, on Mechanical Behavior of Jointed Rock Blocks

To investigate the effect of joint shear stiffness, $\overline{k}_{sj}$, on mechanical behavior of jointed rock blocks adjacent to an underground excavation, the joint shear to normal stiffness ratio was varied from 1/3 to 1/300 through 1/30, whereas the joint normal stiffness value was kept unchanged at $\overline{k}_{nj} = 1.36 \times 10^{10}$ N/m^3. In addition, the other joint micro-mechanical parameter values were also kept constant, i.e. $\overline{\sigma}_{cj} = 0.5$ MPa, $\varphi_j = 20°$,

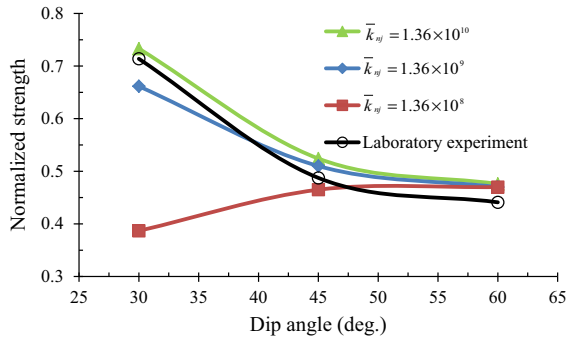

Fig. 11 Comparison of jointed rock block strength between the laboratory experiment and numerical modeling results. (Note that the unit for joint normal stiffness is N/m^3.)

$c_j = 0.5$ MPa, and $\mu_j = 0.3$. Figures 12 and 13 displays, respectively, the failure mode and normalized strength of the jointed rock blocks having different joint shear stiffness values.

Compared to the failure modes and normalized strength of the jointed rock blocks displayed in Figs. 9 and 10, the differences observed in Figs. 12 and 13 mainly happen at $\alpha = 0°$. That means the joint shear stiffness has similar effect as the joint normal stiffness on the jointed rock block behavior except for $\alpha = 0°$. When the non-persistent joints are horizontal ($\alpha = 0°$), the failure mode stays as the intact failure irrespective of the shear stiffness value (see Fig. 12). Therefore, decrease of the shear stiffness has negligible effect on the strength of the jointed rock blocks having horizontal joints.

The dominant roles the joint normal stiffness and joint shear stiffness play on the mechanical behavior of the jointed rock blocks having low to moderate joint dip angles (i.e. $\alpha = 0°$, 15°, 30° and 45°) are explained below. When the joint dip angle is low, a higher component of the vertical loading is shared by the joint segments as the normal stress acts on the joints. Thus, the decrease of the joint normal stiffness should weaken the resistance to deformation of joint segments and transfer more load sharing to intact bridges and influence the mechanical response of the jointed rock blocks under compression. Figure 14 displays the force chain in the jointed rock block having horizontal joints ($\alpha = 0°$) under different joint normal stiffness values at a certain vertical strain level (0.9%) before the peak stress. As shown in Fig. 14a, when the joint normal stiffness is high ($\overline{k}_{nj} = 1.36 \times 10^{10}$ N/m^3), the compression force chains distribute uniformly more or less between the parallel joints as well as the rock bridges. When the joint normal stiffness is low ($\overline{k}_{nj} = 1.36 \times 10^{8}$ N/m^3), the compression force chains mainly concentrate in the vertical columns including less parallel joints (near the left and right edges of the jointed rock block in Fig. 14b). That means the decrease of the joint normal stiffness leads to less load sharing by the joints compared to the rock bridges. Thus, in a vertical jointed rock column having more parallel joints, the rock materials above and below the joints contribute less to the global strength of the jointed rock block. On the other hand, when the joint dip angle is high ($\alpha \geqq 60°$) the normal stress component of the vertical load acting on the joint segments is small; therefore, the change of the joint normal stiffness has negligible effect on the jointed rock block behavior. With respect to the joint shear stiffness, it has negligible influence on the behavior of jointed rock blocks having horizontal joints ($\alpha = 0°$) because there is no shear or slip happening in joints. As the joints become inclined ($\alpha \geqq 15°$), they begin to share the shear stress component of the vertical load. When the joint shear stiffness decreases, which means the joint resistance to loading decreases, the strength of the whole jointed rock block decreases accordingly (examples: $\alpha = 15°$ and 30°) (Fig. 13). When the joint dip angle is large enough (example; $\alpha = 60°$), the shear stress component resulting from the vertical compressive load becomes dominant to break the jointed rock block in a planar failure mode. The rock bridges and joint segments on one joint set plane basically bear the loading stress at the same time (Jennings 1970). However, the shear strength of joint segments is significantly less than that of the rock bridges due to the small normal stress component acting on the joint surfaces according to Eq. 1, as well as due to the low shear strength parameter values ($\varphi_j = 15°$, $c_j = 0.5$ MPa). Therefore, the contribution of joint segments to the whole jointed rock mass is insignificant because of the low joint shear strength. Therefore, the variation of joint shear stiffness plays a negligible role for high joint dip angles such as $\alpha = 60°$ and $\alpha = 75°$ On the other hand, for high dip angles, the joint shear strength parameter values may play important roles on the jointed rock block response. In the following sections, the effect of joint strength parameter values on a jointed rock block behavior adjacent to an underground excavation is systematically investigated.

3.3 Effect of the Bonded Joint Friction Angle, φ_j, on Mechanical Behavior of Jointed Rock Blocks

To learn about the effect of the joint shear strength on mechanical behavior of jointed rock blocks adjacent to an underground excavation, the effect of the joint shear strength parameters: the bonded joint friction angle, φ_j, cohesion, c_j, and joint friction coefficient, μ_j, on jointed rock block behavior is investigated based on the particle flow model shown in Fig. 3. First, the effect of φ_j on the failure mode and strength of the

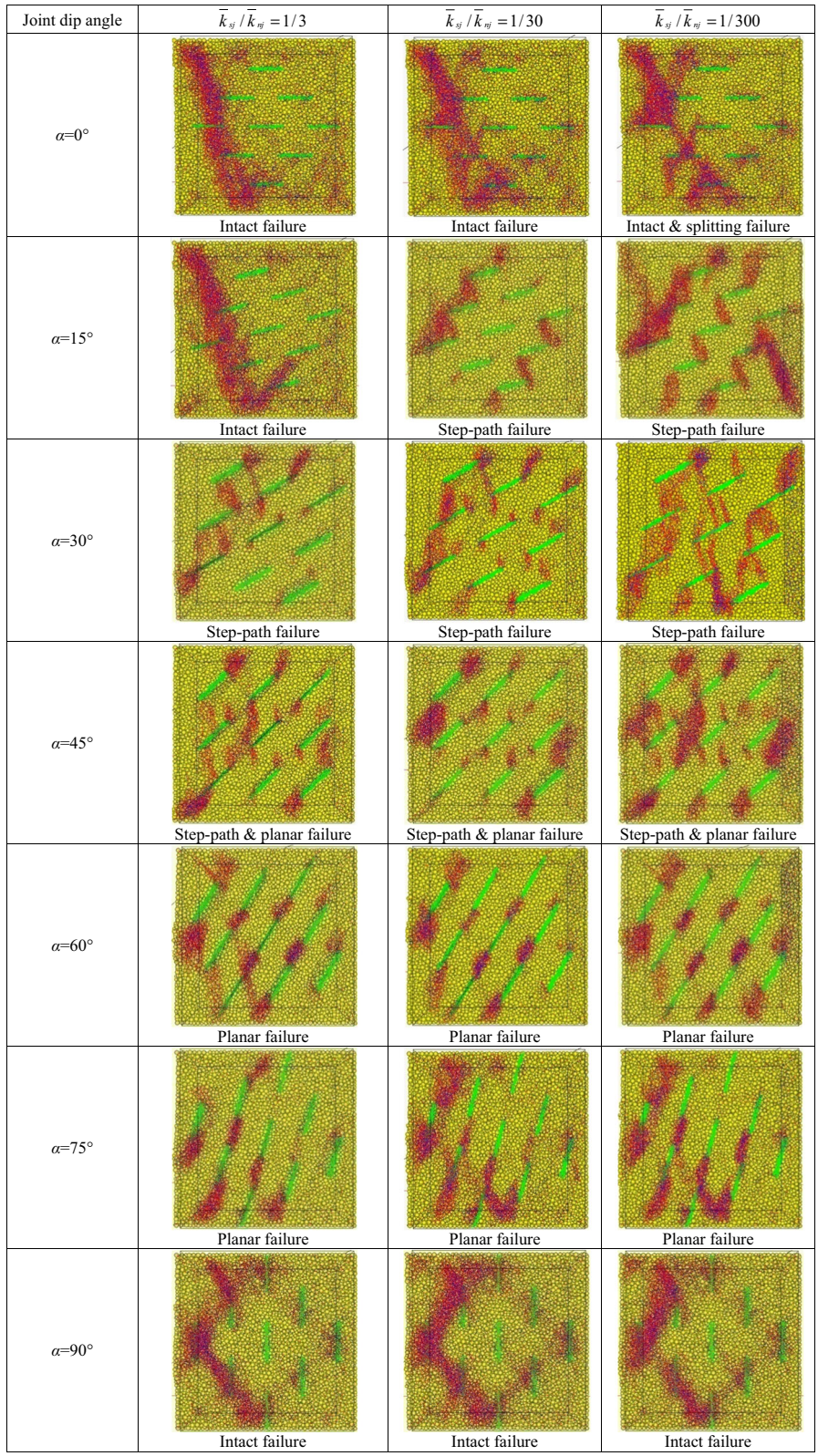

Fig. 12 Failure modes of the jointed rock blocks having different joint dip angles and joint shear stiffness. (Note that the free surface is on the left-hand side of each block.)

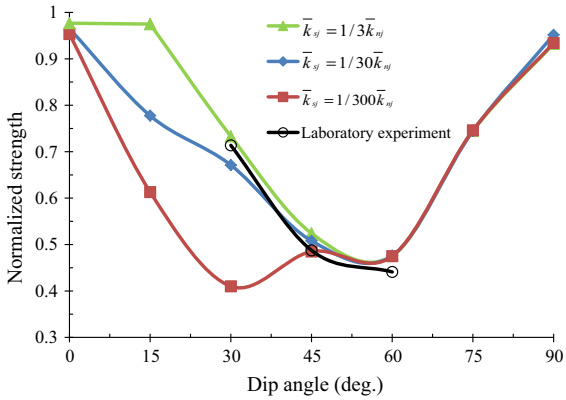

Fig. 13 Normalized strength of the jointed rock blocks having different joint shear stiffness

jointed rock blocks is analyzed. The bonded joint friction angle was varied from 20° to 40° through 30°, while the other joint micro-mechanical parameters were kept constant, i.e. $\overline{k}_{nj} = 1.36 \times 10^{10}$ N/m^3, $\overline{k}_{sj}/\overline{k}_{nj} = 1/3$, $\overline{\sigma}_{cj} = 0.5$ MPa, $c_j = 0.5$ MPa, and $\mu_j = 0.3$. Figures 15 and 16 displays, respectively, the failure mode and normalized strength of the jointed rock blocks having different bonded joint friction angle.

According to Fig. 15, when the bonded joint friction angle varies from 20° to 40° through 30°, the failure mode of the jointed rock blocks with a certain joint orientation angle changes. For $\alpha = 30°$, the failure mode of the jointed rock blocks changes from the step-path failure to intact failure as the bonded joint friction angle increases. As a result, the normalized strength value increases from 0.733 to 0.935 (Fig. 16). In addition, with the increase of the bonded joint friction angle, the failure mode changes from the step-path and planar failure to planar failure for $\alpha = 45°$. The increase of the bonded joint friction angle prevents the appearance of the step-path failure mode adjacent to the free surface. This change of the failure mode also increases the normalized strength of the jointed rock blocks, from 0.524 to 0.723 through 0.567, as shown in Fig. 16. For $\alpha = 60°$, even though the failure mode of the jointed rock blocks is almost the same, the strength is improved slightly with the increase of the bonded joint friction angle. However, the improvement of the jointed rock block strength is not significant, only from 0.476 to 0.491 through 0.478. For dip angle of 75°, both the mode of failure and the jointed rock block strength remains the same irrespective of the value of the bonded joint friction angle.

Therefore, the bonded joint friction angle has significant to negligible influence on the mechanical behavior of the jointed rock blocks as the joint dip angle varies from 30° to 75°. With respect to the jointed rock blocks with dip angles of 0°, 15° and 90°, no difference was observed. This is because the jointed

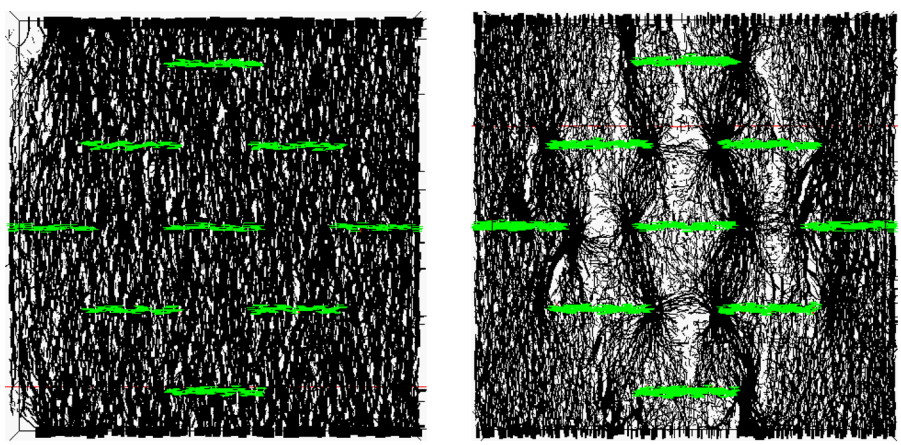

(a) **(b)**

Fig. 14 Force chains in the jointed rock block having horizontal joints under different joint normal stiffness at an applied vertical strain of 0.9%. Note that the black chain and red chain imply compression force and tension force, respectively, and the force quantity is proportional to the chain thickness. (Note that the free surface is on the left-hand side of each block.). **a** $\overline{k}_{nj} = 1.36 \times 10^{10}$ N/m^3. **b** $\overline{k}_{nj} = 1.36 \times 10^{8}$ N/m^3

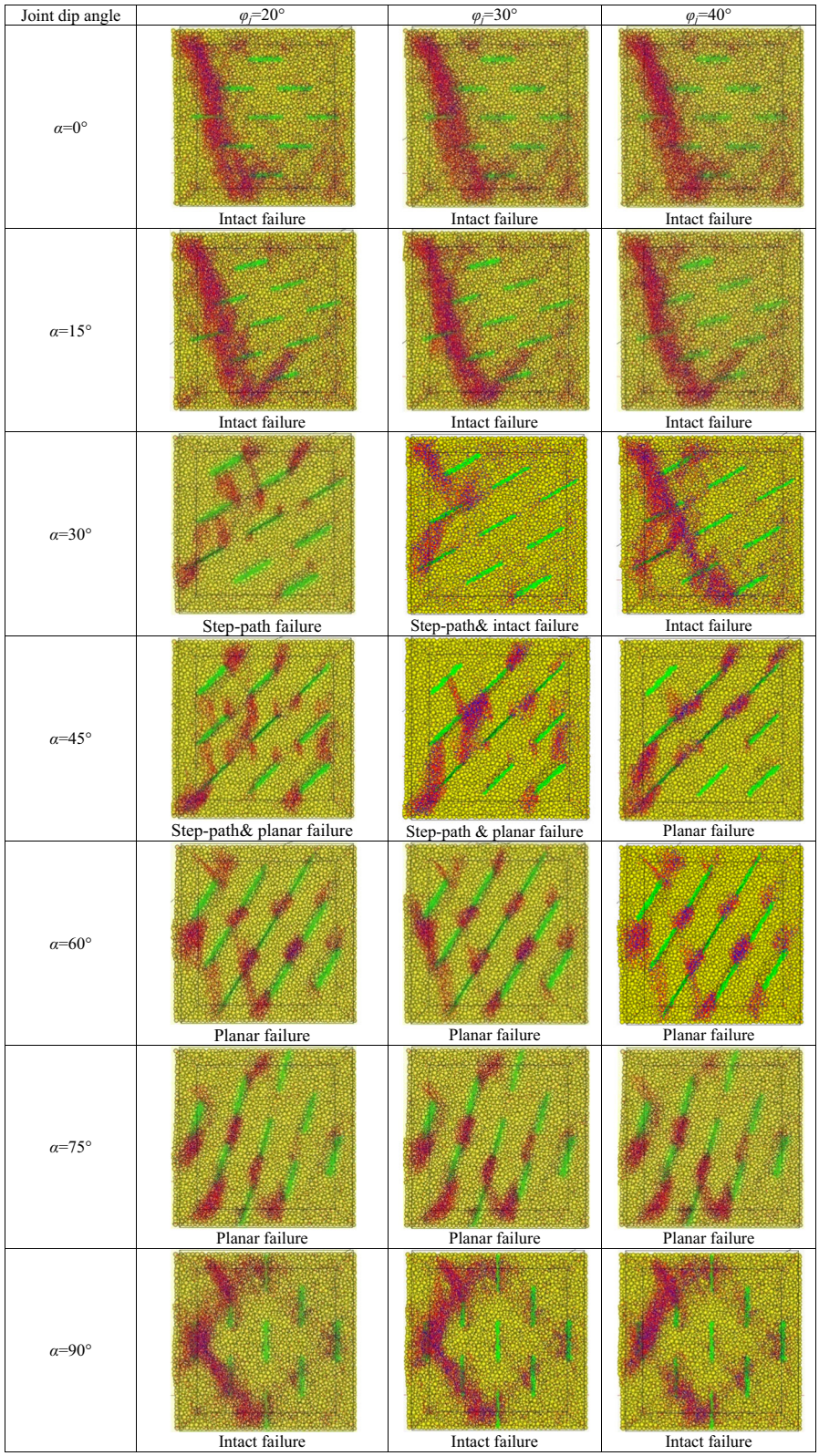

Fig. 15 Failure modes of the jointed rock blocks having different bonded joint friction angle. (Note that the free surface is on the left-hand side of each block.)

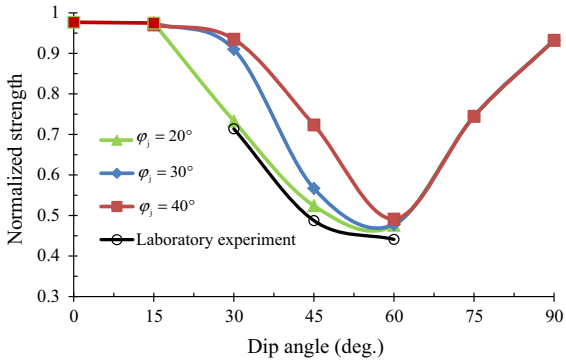

Fig. 16 Normalized strength of the jointed rock blocks having different bonded joint friction angle

rock blocks fail in the intact failure mode regardless of the variation of the bonded joint friction angle. For dip angles of 30° to 75°, both the strength of the joints and the strength of the intact rock bridges contribute to the jointed block strength. Therefore, increase of the bonded joint friction angle should lead to increase of the strength of the jointed rock blocks. Nevertheless, when the joint dip angle is high (examples: $\alpha = 60°$ and 75°), the normal stress component, $\overline{\sigma}_{nj}$, acting on the joints is quite small. Accordingly, the joint shear strength, $\overline{\tau}_{nj}$, increases very little according to Eq. 1 due to the increase of the bonded joint friction angle. Therefore, the jointed block strength increases negligibly with the increase of the bonded joint friction angle. The effect of the bonded joint friction angle on jointed rock block behavior depends heavily on the normal and shear stress components acting on the joint surfaces.

3.4 Effect of the Bonded Joint Cohesion, c_j, on Mechanical Behavior of Jointed Rock Blocks

To understand the effect of joint shear strength on mechanical behavior of jointed rock blocks adjacent to an underground excavation, the effect of the bonded joint cohesion, c_j, on mechanical behavior of jointed rock blocks is investigated in this section. The bonded joint cohesion, c_j, was varied from 0.5 to 1.5 MPa through 1.0 MPa, whereas the other joint micro-mechanical parameter values were kept constant, i.e. $\overline{k}_{nj} = 1.36 \times 10^{10}$ N/m^3, $\overline{k}_{sj}/\overline{k}_{nj} = 1/3, \overline{\sigma}_{cj} = 0.5$ MPa, $\varphi_j = 20°$, and $\mu_j = 0.3$. Figures 17 and 18 displays, respectively, the failure mode and normalized strength of the jointed rock blocks having different bonded cohesion.

Figure 17 demonstrates the variation of the jointed rock block failure mode with respect to relatively high dip angles, i.e. $\alpha = 30°$, $\alpha = 45°$, 60°, 75° and 90°. With the increase of the bonded joint cohesion, the failure mode of the jointed rock block with dip angle of 30° changes from step-path failure to intact failure through step-path and intact failure. With the increase of the bonded joint cohesion, the failure mode of the jointed rock block with dip angle of 45° changes from step-path and planar failure to planar and intact failure through planar failure. That means the increase of the bonded joint cohesion not only prevents sliding on the joint adjacent to the free surface, but also blocks partly the sliding on the joints in the inner part of the jointed rock block. For $\alpha = 60°$, although the failure mode is the same, the increase of the bonded joint cohesion induces more fractures around the joints (see elliptical areas in Fig. 17 at $\alpha = 60°$). For $\alpha = 75°$, the failure mode changes from planar failure to planar and intact failure and the possible planar failure only gets limited adjacent to the free surface. When the joints are vertical ($\alpha = 90°$) the development path of macro failure plane transforms generally to be like that of the intact rock block (Fig. 8). With the increase of the bonded joint cohesion, the effect of the joint located closest to the free surface (the most left one) on the failure mode of the jointed rock block basically gets eliminated.

The normalized strength of the jointed rock blocks increases with the increase of the bonded joint cohesion as shown in Fig. 18. Increase of the bonded joint friction angle contributed to the strength increase of the jointed rock blocks with dip angles of 30° and 45° (Fig. 16). The increase of the bonded joint cohesion not only improved the strength of the jointed blocks with dip angles of 30° and 45°, but also improved the strength of the jointed rock blocks with dip angles of 60°, 75° and 90° as well. The increase of the normalized strength value for $\alpha = 60°$ is the most dramatic, from 0.476 to 0.952 through 0.727. For $\alpha = 75°$, the normalized strength of the jointed rock blocks increased from 0.745 to 0.973 through 0.886. In addition, for $\alpha = 90°$, with the increase of the bonded joint cohesion, the normalized strength increased from 0.932 to 0.977 through 0.971. Contrary to the bonded joint friction angle, increase of the bonded joint cohesion directly works on increasing the joint shear

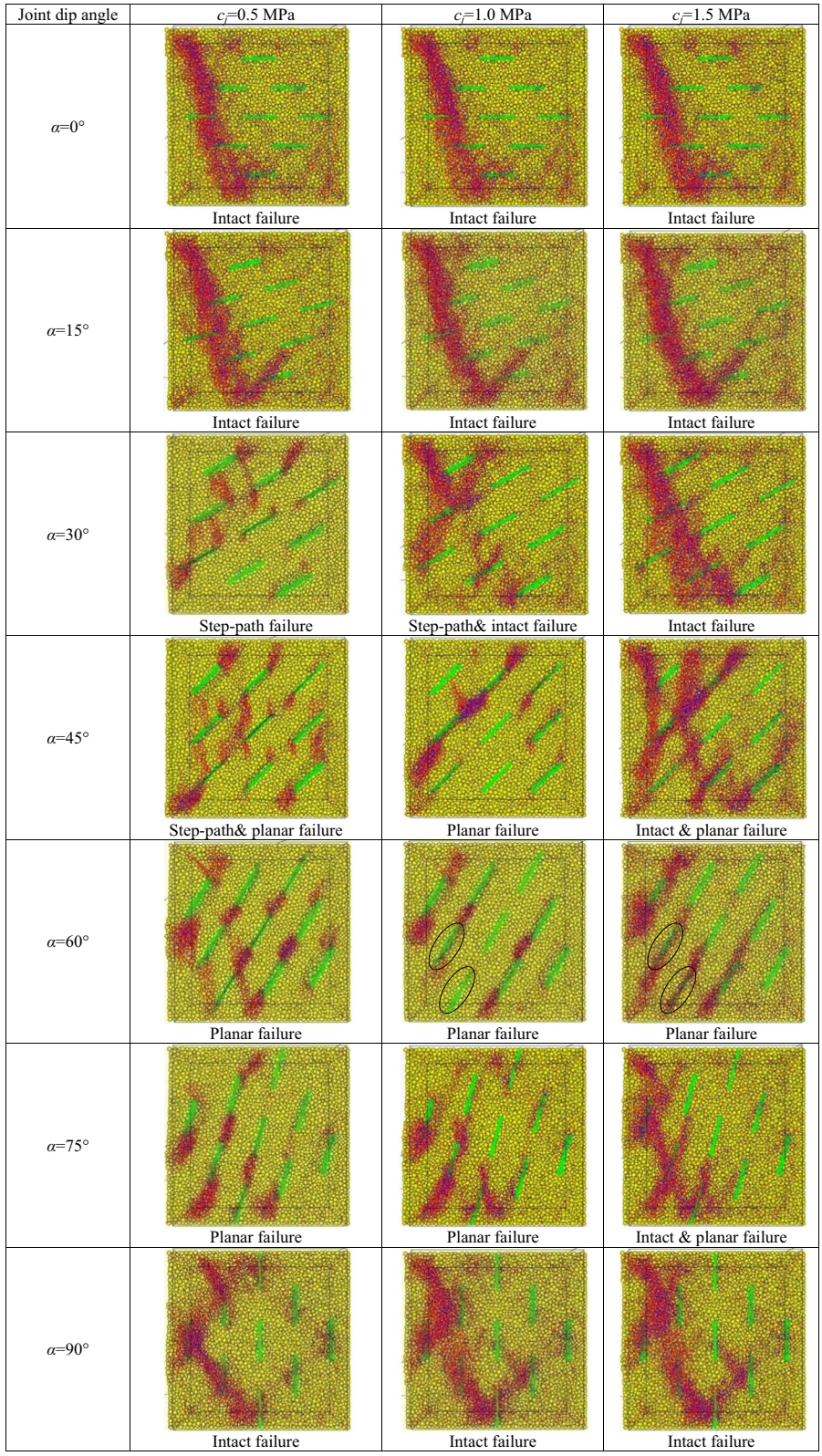

Fig. 17 Failure modes of the jointed rock blocks having different bonded joint cohesion. (Note that the free surface is on the left-hand side of each block.)

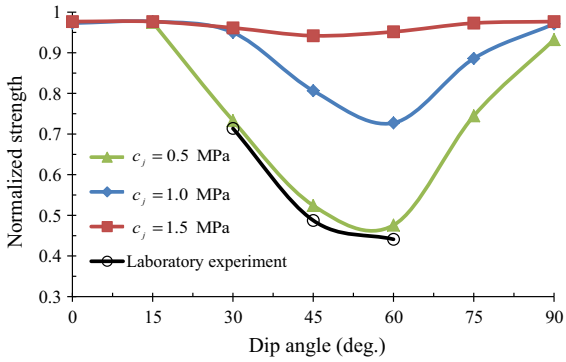

Fig. 18 Normalized strength of jointed rock blocks having different bonded joint cohesion

strength with no dependence on the normal stress component acting on the joint surfaces. That is the reason why the variation of the bonded joint cohesion rather than the bonded joint friction angle can improve the jointed block strength for α = 60°, 75° and 90°.

3.5 Effect of the Joint Friction Coefficient, μ_j, on Mechanical Behavior of Jointed Rock Blocks

The joint friction coefficient begins to work only after the joint bond breaks to provide the residual shear strength. To learn about the effect of joint residual shear strength on mechanical behavior of jointed rock blocks adjacent to an underground excavation, the effect of the joint friction coefficient, μ_j, on mechanical behavior of jointed rock blocks is investigated in this section. The joint friction coefficient was varied from 0.10 to 0.30 through 0.20,which is all less than the bonded joint friction coefficient ($\varphi_j = 20°$, tan 20° = 0.325). On the other hand, the other joint micro-mechanical parameter values were kept unchanged, i.e. $\overline{k}_{nj} = 1.36 \times 10^{10}$ N/m^3, $\overline{k}_{sj}/\overline{k}_{nj} = 1/3$,$\overline{\sigma}_{cj} =$ 0.5 MPa, $\varphi_j = 20°$ and $c_j = 0.5$ MPa. Figures 19 and 20 displays, respectively, the failure mode and normalized strength of the jointed rock blocks having different joint friction coefficient.

As shown in Figs. 19 and 20, for dip angles 15° through 60°, the joint friction coefficient has slight to moderate effect on the failure mode and strength behavior of jointed rock blocks. Like the bonded joint friction angle, the increase of the joint friction coefficient prevents to some extent shearing on the joint adjacent to the free surface and thereby influences the failure mode of the jointed rock blocks. For example, for α = 15°, the failure mode changes from the step-path and intact failure to intact failure with the increase of the joint friction coefficient. Shearing on joints is an important component to produce the step-path failure mode and planar failure mode. Accordingly, the normalized strength of the jointed rock blocks with dip angles of 30°, 45° and 60° more or less improves slightly with the increase of the joint friction coefficient, even though the failure mode is unchanged for these cases. When the joint dip angle is high enough (example: α = 75°), the effect of the joint friction coefficient on jointed rock block behavior becomes negligible, because the increase of the joint shear strength through modifying μ_j also has dependence on the normal stress component acting on the joint surfaces. To some extent, μ_j has a similar effect compared to that of φ_j on the global behavior of jointed rock blocks. If φ_j is lower, the failure mode and strength should be more sensitive to the variation of μ_j.

A sensitivity study on the effect of the joint tensile strength, $\overline{\sigma}_{cj}$, on jointed rock block behavior was undertaken as well by changing this joint micro-mechanical parameter from 0.5 to 1.5 MPa through 1.0 MPa while keeping the other parameter values unchanged. The numerical results showed that the variation of the joint tensile strength has negligible effect on the jointed rock block failure mode. In addition, it has almost no influence on the normalized strength of the jointed rock blocks apart from the one having 90° dip angle, as demonstrated in Fig. 21.

4 Effect of Shear and Slip of Joints on Jointed Rock Block Behavior

According to the aforesaid numerical modeling results, it turns out that the joint shear strength parameters which are the bonded joint friction angle, bonded joint cohesion and joint friction coefficient have more influence than the joint tensile strength on mechanical behavior of jointed rock blocks adjacent to an underground excavation. To explain the mechanism behind this phenomenon, the mechanical response of the joints in rock block models under compression as well as their effect on the whole jointed rock block behavior are further analyzed in this section.

Joint dip angle	μ_j=0.10	μ_j =0.20	μ_j =0.30
α=0°	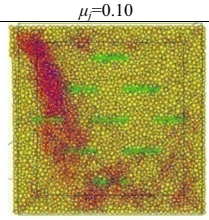 Intact failure	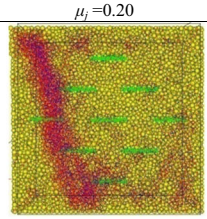 Intact failure	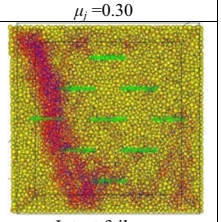 Intact failure
α=15°	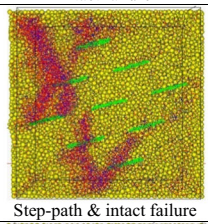 Step-path & intact failure	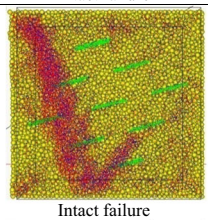 Intact failure	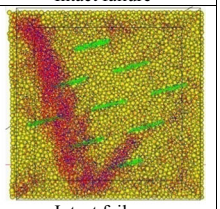 Intact failure
α=30°	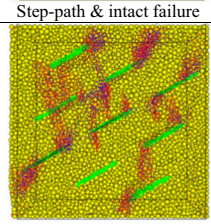 Step-path	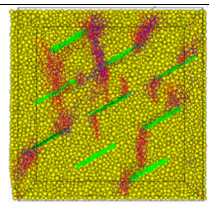 Step-path	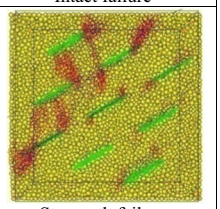 Step-path failure
α=45°	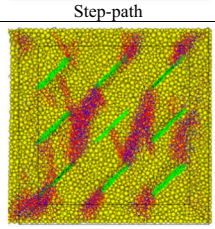 Step-path & planar failure	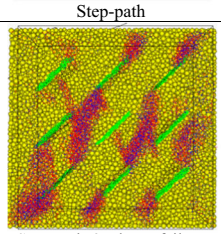 Step-path & Planar failure	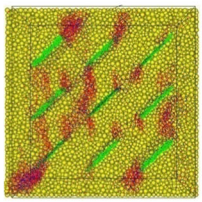 Step-path& planar failure
α=60°	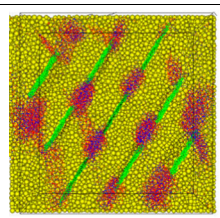 Planar failure	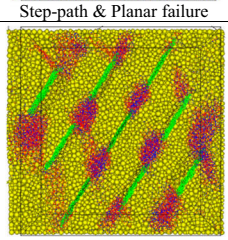 Planar failure	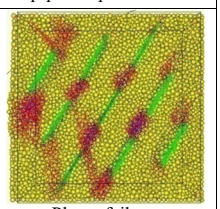 Planar failure
α=75°	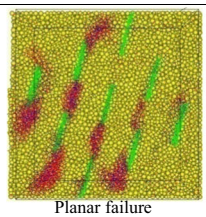 Planar failure	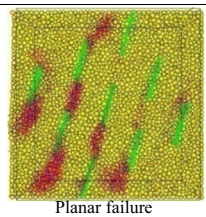 Planar failure	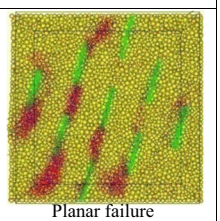 Planar failure
α=90°	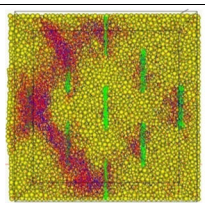 Intact failure	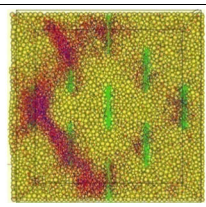 Intact failure	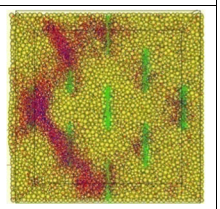 Intact failure

Fig. 19 Failure modes of the jointed rock blocks having different joint friction coefficient. (Note that the free surface is on the left-hand side of each block.)

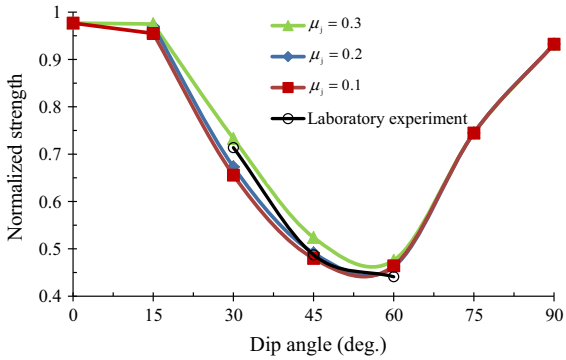

Fig. 20 Normalized strength of the jointed rock blocks having different joint friction coefficient

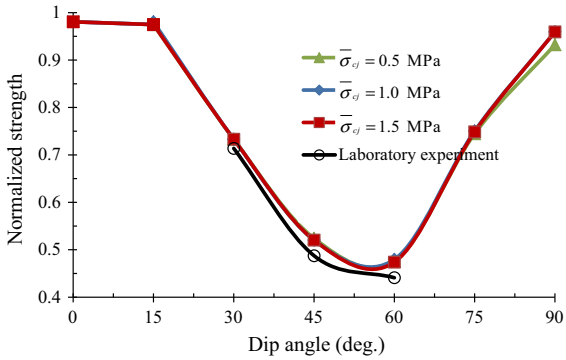

Fig. 21 Normalized strength of the jointed rock blocks having different joint tensile strength

As we know, a joint bond can break either in the tensile mode or shear mode to produce correspondingly either a tensile or a shear fracture (Itasca Consulting Group Inc. 2008). This means that the appearance of a tensile fracture or shear fracture in a bonded joint can reflect the mechanical response of the joint surfaces to some extent. Figure 22 displays the variation of the number of micro fractures with the vertical strain (in σ_1 direction) in the joint segments during the numerical compression tests. Note that the joint micro-mechanical parameter values used herein are the same for all the jointed rock blocks, i.e. $\overline{k}_{nj} = 1.36 \times 10^{10}$ N/m^3, $\overline{k}_{sj}/\overline{k}_{nj} = 1/3$, $\overline{\sigma}_{cj} = 0.5$ MPa, $\varphi_j = 20°$, $c_j = 0.5$ MPa, and $\mu_j = 0.3$. As shown in Fig. 22, there are more shear bond breakages (shear fractures) than the tensile bond breakages (tensile fractures) in the joint segments regardless of the joint dip angle. The number of tensile fractures is small for all cases except for the jointed rock block with the vertical joints ($\alpha = 90°$). On the contrary, the number of shear fractures experiences a significant rise during the test, especially for the jointed rock blocks with dip angles of 30°, 45°, 60° and 75°. This means that the shear and slip mechanisms of the joint surfaces drive the generation of micro shear fractures when the jointed rock blocks are tested under compression. Apparently, the shear and slip response of the joints are the dominant factors affecting the mechanical behavior of the jointed rock blocks.

Furthermore, as shown in Fig. 23, the shear and slip response of joints also influence the strength of the jointed rock blocks. This figure displays the relation between the number of joint shear fractures and the normalized strength of the jointed rock blocks having different joint orientations. Note that for each jointed block the number of joint shear fractures is obtained when the peak stress is reached. As shown in Fig. 23, the low numbers of joint shear fractures correspond to the high normalized strength values of the jointed rock blocks; while the high numbers of joint shear fractures correspond to the low normalized strength values of the jointed rock blocks. For instance, for $\alpha = 0°$, the number of joint shear fractures is 115, and the normalized strength value is as high as 0.977, which is quite close to the intact rock block strength. While for $\alpha = 60°$, the number of joint shear fractures is 12,170, and the corresponding normalized strength value is only 0.476. Therefore, it can be concluded that the shear and slip response of joints weaken the resistance capacity of a jointed rock block. It also explains why the increase of the joint shear strength significantly increases the strength of a jointed rock block having non-persistent joints.

5 Conclusions

Numerical simulation using particle flow approach was utilized to investigate the effect of infilled joint micro-mechanical parameters on the mechanical behavior of jointed rock blocks adjacent to an underground excavation. After setting up a particle flow model with the PFC^{3D} software package according to the conceptual model proposed by Zhang (2013) and Jing et al. (2014), a parametric study was undertaken to investigate the effect of the joint normal stiffness, joint shear stiffness, bonded joint friction angle, bonded joint cohesion, joint friction coefficient as well as the joint tensile strength on the failure mode

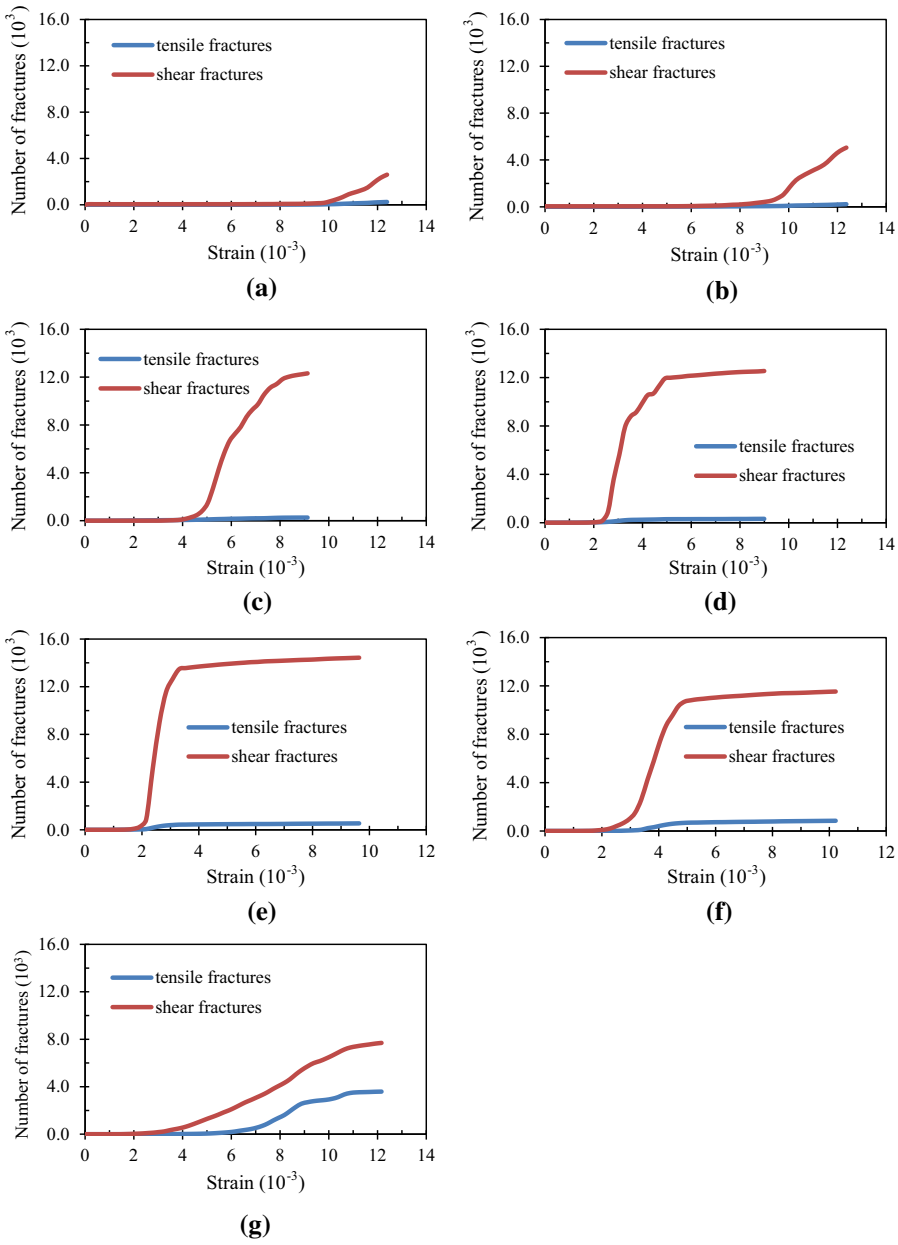

Fig. 22 Number of micro fractures captured in joint segments. **a** $\alpha = 0°$. **b** $\alpha = 15°$. **c** $\alpha = 30°$. **d** $\alpha = 45°$. **e** $\alpha = 60°$. **f** $\alpha = 75°$. **g** $\alpha = 90°$

and strength of rock blocks having non-persistent joints. The following conclusions can be drawn from the obtained numerical simulation results:

1. Four basic failure modes were identified in the jointed rock blocks: (a) intact material failure mode, (b) splitting failure mode, (c) step-path failure mode and (d) planar failure mode. Some of the failure images indicated the possibility of having different combinations of two of the failure modes (examples: step-path and planar; step-path and intact; planar and intact; intact and splitting).
2. The joint normal stiffness mainly affects the mechanical behavior of the jointed rock blocks having low to moderate joint dip angles, such as $\alpha = 0°$, 15°, 30° and 45°. The increase of the joint normal stiffness increases the normalized strength of the jointed rock blocks with joint dip angles less than or equal to 45°.

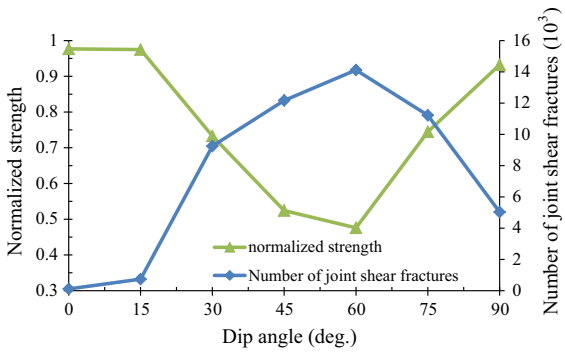

Fig. 23 Relation between the normalized strength and the number of joint shear fractures

3. Apart from $\alpha = 0°$, for other joint orientations, the effect of the joint shear stiffness on the mechanical behavior of the jointed rock blocks seems to be like that of the joint normal stiffness.
4. The bonded joint friction angle has a pronounced effect on the mechanical response of jointed rock blocks having dip angles of 30° and 45°. As the joint dip angle increases (examples: $\alpha = 60°$ through 90°), the effect of the bonded joint friction angle becomes negligible due to the low normal stress component acting on the joint surfaces.
5. The joint friction coefficient seems to have only a slight effect on the mechanical response of jointed rock blocks having dip angles of 30°, 45° and 60°. For jointed blocks having other dip angles, the effect of the joint friction coefficient on the mechanical response of the jointed blocks seems negligible.
6. The increase of the bonded joint cohesion directly increases the joint shear strength and thus increases the strength of jointed rock blocks having inclined joints even up to 75°.
7. The joint tensile strength seems to have no effect on the failure mode or strength of the jointed rock blocks having dip angles less than or equal to 75°. Increase of the joint tensile strength increases slightly the strength of the jointed blocks having 90° dip angle.
8. The applied stress path resulted in more shear fractures compared to the tensile fractures. This means that the joint micro-mechanical parameters that can increase the joint shear strength such as the bonded joint cohesion and bonded joint friction angle play major roles in increasing the strength of jointed blocks having almost all the dip angles.
9. The results indicated the importance of using proper micro-mechanical parameter values to obtain realistic behavior of jointed rock masses in investigating stability of underground excavations using PFC^{3D}.

Acknowledgements The research reported in this paper was financially supported by the State Key Laboratory for Geomechanics and Deep Underground Engineering, China University of Mining and Technology Contract (No. SKLGDUEK1416) given to the second author. The research was also partially funded by the NIOSH of the Centers for Disease Control and Prevention, USA through Contract No. 200-2011-39886 given to the second author. This research was also partially supported by the National Natural Science Foundation of China (Grant No. 51704183) and the Natural Science Foundation of Shandong Province (Grant No. ZR2017BEE020).

References

Bahaaddini M, Sharrock G, Hebbelwhite B, Mitra R (2012) Direct shear tests to model the shear behaviour of rock joints by PFC2D. In: 46th US rock mechanics/geomechanics symposium, Chicago, USA

Bahaaddini M, Sharrock G, Hebblewhite BK (2013) Numerical investigation of the effect of joint geometrical parameters on the mechanical properties of a non-persistent jointed rock mass under uniaxial compression. Comput Geotech 49:206–225

Bahaaddini M, Hagan PC, Mitra R, Hebblewhite BK (2015) Parametric study of smooth joint parameters on the shear behavior of rock joints. Rock Mech Rock Eng 48:923–940

Barton N, Bandis S, Bakhtar K (1985) Strength, deformation and conductivity coupling of rock joints. Int J Rock Mech Min Sci Geomech Abstr 22(3):121–140

Chen PY (2017) Effects of microparameters on macroparameters of flat-jointed bonded-particle materials and suggestions on trial-and-error method. Geotech Geol Eng 35:663–677

Fan X, Kulatilake PHSW, Chen X (2015) Mechanical behavior of rock-like jointed blocks with multi-non-persistent joints under uniaxial loading: a particle mechanics approach. Eng Geol 190:17–32

Ghazvinian A, Sarfarazi V, Schubert W, Blumel M (2012) A study of the failure mechanism of planar non-persistent open joints using PFC2D. Rock Mech Rock Eng 45:677–693

Hu WR, Kwok CY, Duan K, Wang T (2018) Parametric study of the smooth-joint contact model on the mechanical behavior of jointed rock. Int J Numer Anal Methods Geomech 42:358–376

Huang D, Wang J, Liu S (2015) A comprehensive study on the smooth joint model in DEM simulation of jointed rock masses. Granul Matter 17(6):775–791

Indraratna B, Aziz NI, Dey A (2001) Behavior of joints containing clay infill under constant normal stiffness, with and without bolting. Geotech Eng 149(4):259–267

Itasca Consulting Group Inc. (1995) PFC3D-Particle flow code in 3-dimensions, version 1.1, user's manual, vol. I and II, Minneapolis

Itasca Consulting Group Inc. (2008) PFC3D–particle flow code in 3-dimensions, version 4.0., user's manual, Minneapolis

Jamil SM (1992) Strength of non-persistent rock joints. PhD thesis. Urbana, Illinois: University of Illinois

Jennings JE (1970) A mathematical theory for the calculation of the stability of open cast mines. In: Proceedings of the symposium on theoretical background to the planning of open pit mines, Johannesburg, pp 87–102

Jing HW, Yang SQ, Zhang ML, Xu GA, Kunfu Chen (2014) An experimental study on anchorage strength and deformation behavior of large-scale jointed rock mass. Tunn Undergr Space Technol 43:184–197

Kim BH, Cai M, Kaiser PK, Yang HS (2007) Estimation of block sizes for rock masses with non-persistent joints. Rock Mech Rock Eng 40(2):169–192

Kulatilake PHSW, Wang S, Stephansson O (1993) Effect of finite size joints on deformability of jointed rock at the three-dimensional level. Int J Rock Mech Min Sci 30(5):479–501

Kulatilake PHSW, Malama B, Wang J (2001) Physical and particle flow modeling of jointed rock block behavior under uniaxial loading. Int J Rock Mech Min Sci 43:641–657

Lee H, Jeon S (2011) An experimental and numerical study of fracture coalescence in pre-cracked specimens under uniaxial compression. Int J Solids Struct 48:979–999

Mars Ivars D, Pierce ME, Darcel C, Reyes-Montes J, Potyondy DO, Young RP, Cundall PA (2011) The synthetic rock mass approach for jointed rock mass modelling. Int J Rock Mech Min Sci 48:219–244

Mehranpour MH, Kulatilake PHSW (2016) Comparison of six major intact rock criteria using a particle flow approach under true triaxial stress conditions. Int J Geomech Geophys Geoenergy Georesour 2:203–229

Mehranpour HM, Kulatilake PHSW (2017) Improvements for smooth joint contact model of the particle flow code and its applications. Comput Geotech 87:163–177

Potyondy DO, Cundall PA (2004) A bonded-particle model for rock. Int J Rock Mech Min Sci 41(8):1329–1364

Prudencio M, Van Sint Jan M (2007) Strength and failure modes of rock mass models with non-persistent joints. Int J Rock Mech Min Sci 44(6):890–902

Sarfarazi V, Ghazvinian A, Schubert W, Blumel M, Nejati HR (2014) Numerical simulation of the process of fracture of echelon rock joints. Rock Mech Rock Eng 47:1355–1371

Tien YM, Kuo MC, Juang CH (2006) An experimental investigation of the failure mechanism of simulated transversely isotropic rocks. Int J Rock Mech Min Sci 43:1163–1181

Wu Q, Kulatilake PHSW (2012) REV and its properties on fracture system and mechanical properties, and an orthotropic constitutive model for a jointed rock mass in a dam site in China. Comput Geotech 43:124–142

Yang B, Jiao Y, Lei S (2006) A study on the effects of micro parameters on macro properties for specimens created by bonded particles. Eng Comput 23(6):607–631

Yang XX, Kulatilake PHSW, Jing HW, Yang SQ (2015) Numerical simulation of a jointed rock block mechanical behavior adjacent to an underground excavation and comparison with physical model test results. Tunn Undergr Space Technol 50:129–142

Yin DW, Meng XX (2018) Numerical simulation on uniaxial compression failure of a roof rock-coal-floor rock composite sample with coal persistent joint. Geotech Geol Eng. https://doi.org/10.1007/s10706-018-0585-9

Zhang ML (2013) Research on crack evolution and bolting mechanism of intermittently jointed rocks. PhD thesis. China University of Mining and Technology, Xuzhou, China

Zhang Y, Stead D (2014) Modelling 3D crack propagation in hard rock pillars using a synthetic rock mass approach. Int J Rock Mech Min Sci 72:199–213

Zhang XP, Wong LNY (2012) Cracking process in rock-like material containing a single flaw under uniaxial compression: a numerical study based on parallel bonded-particle model approach. Rock Mech Rock Eng 45:711–737

Zhang XP, Wong LNY (2013) Crack initiation, propagation and coalescence in rock-like material containing two flaws: a numerical study based on bonded-particle model approach. Rock Mech Rock Eng 46:1001–1021

Zhao WH, Huang RQ, Yan M (2015) Study on the deformation and failure modes of rock mass containing concentrated parallel joints with different spacing and number based on smooth joint model in PFC. Arab J Geosci 8:7887–7897